Active faulting in the Birjand region of NE Iran

R. T. Walker[1] and M. M. Khatib[2]

Received 21 June 2005; revised 9 January 2006; accepted 15 May 2006; published 17 August 2006.

[1] We use satellite imagery and field observations to investigate the distribution of active faults around Birjand in eastern Iran to determine how the transition between conjugate zones of faulting can be accommodated by diffuse active faulting. In the south of the study area, right-lateral strike-slip faults of the Sistan Suture Zone end in thrusts which die away westward from the strike-slip faults. These thrust terminations appear to allow a northward change to E-W thrusting in central parts of the study area. The introduction of E-W thrusting is, in turn, likely to facilitate a change to E-W left-lateral faulting north of the study region. The relatively diffuse pattern of active faulting at Birjand relates to the regional transition between N-S and E-W strike-slip faulting in northeast Iran, which involves a change from nonrotational to rotational deformation. The change from N-S to E-W faulting is likely to result from the orientation of preexisting structures in Iran and western Afghanistan, which are roughly parallel to the active fault zones. The features described at Birjand also show the influence of preexisting structure on the location and style of active faulting at a local scale, with the position of individual faults apparently controlled by inherited geological weaknesses. Very few modern earthquakes have occurred in the region of Birjand and yet destructive events are known from the historical record. The large number of active faults mapped in this study pose a substantial seismic hazard to Birjand and surrounding regions. **Citation:** Walker, R. T., and M. M. Khatib (2006), Active faulting in the Birjand region of NE Iran, *Tectonics*, *25*, TC4016, doi:10.1029/2005TC001871.

1. Introduction

[2] In this paper we describe the active faulting in an area centered on the city of Birjand in Khorassan province of eastern Iran (Figure 1). Birjand is situated in a region of Range-and-Basin topography between the Dasht-e Lut desert in the south and the E-W mountain ranges north of the Doruneh fault (e.g., Figure 1), that is known historically as Qohestan [*LeStrange*, 1905]. We discuss the significance of the faulting near Birjand for descriptions of the local seismic hazard (as the present-day activity of many of the faults has not previously been described), for the regional tectonics, and also more generally, for studies of the ways in which large active continental fault systems interact and evolve over long periods of time.

[3] Our study area is situated in a region of conjugate strike-slip faulting (Figure 1). To the south are the N-S right-lateral faults of the Sistan Suture Zone [e.g., *Freund*, 1970; *Tirrul et al.*, 1983; *Berberian et al.*, 1999, 2000; *Walker and Jackson*, 2004]. In the north, the dominant structures are the E-W left-lateral Dasht-e Bayaz and Doruneh faults [e.g., *Ambraseys and Tchalenko*, 1969; *Berberian and Yeats*, 1999; *Walker et al.*, 2004]. Both of these fault systems accommodate the same N-S right-lateral shear between central parts of Iran and Afghanistan, with the E-W left-lateral Dasht-e Bayaz and Doruneh faults doing so by rotating clockwise about a vertical axis [e.g., *Jackson and McKenzie*, 1984; *Walker and Jackson*, 2004; *Walker et al.*, 2004; *Allen et al.*, 2006] (also see Figure 1).

[4] Large strike-slip faults are found in many regions of active continental shortening [e.g., *Molnar and Tapponnier*, 1975] and are important elements in accommodating tectonic strain, either by allowing the lateral escape of crustal material from the collision zone, as is the case in Turkey [e.g., *McKenzie*, 1972]; by spatially separating (''partitioning'') oblique convergence into strike-slip and shortening components as in the Zagros mountains of southwestern Iran [e.g., *Talebian and Jackson*, 2002]; or by accommodating tectonic shortening by vertical axis rotation of crustal material [e.g., *England and Molnar*, 1990; *Schermer et al.*, 1996].

[5] As movement on strike-slip faults does not always involve simple lateral movements of crustal material, the patterns of faulting can be relatively complex, and may evolve rapidly, with slip orientations that may not be obvious to infer from the overall convergence direction alone [e.g., *McKenzie and Jackson*, 1983; *Jackson and Molnar*, 1990; *Schermer et al.*, 1996]. Relatively little is known about how faults interact with one another in such regions, as a complete understanding would require detailed information not only about the major strike-slip faults themselves but also about the distributed deformation in the crustal blocks surrounding them, information which is very difficult to gather in most regions of active deformation, as small-scale active faults are difficult to identify in the landscape or geology.

[6] Understanding how faults interact in regions involving vertical axis rotations of crustal material is important in order to determine whether the rotations are accommodated by rigid blocks separated by a few major faults [e.g., *Molnar and Tapponnier*, 1975] or by a diffuse faulting throughout a continuously deforming medium [e.g., *England and*

[1]Department of Earth Sciences, University of Oxford, Oxford, UK.
[2]Department of Geology, University of Birjand, Birjand, Iran.

0278-7407/06/2005TC001871

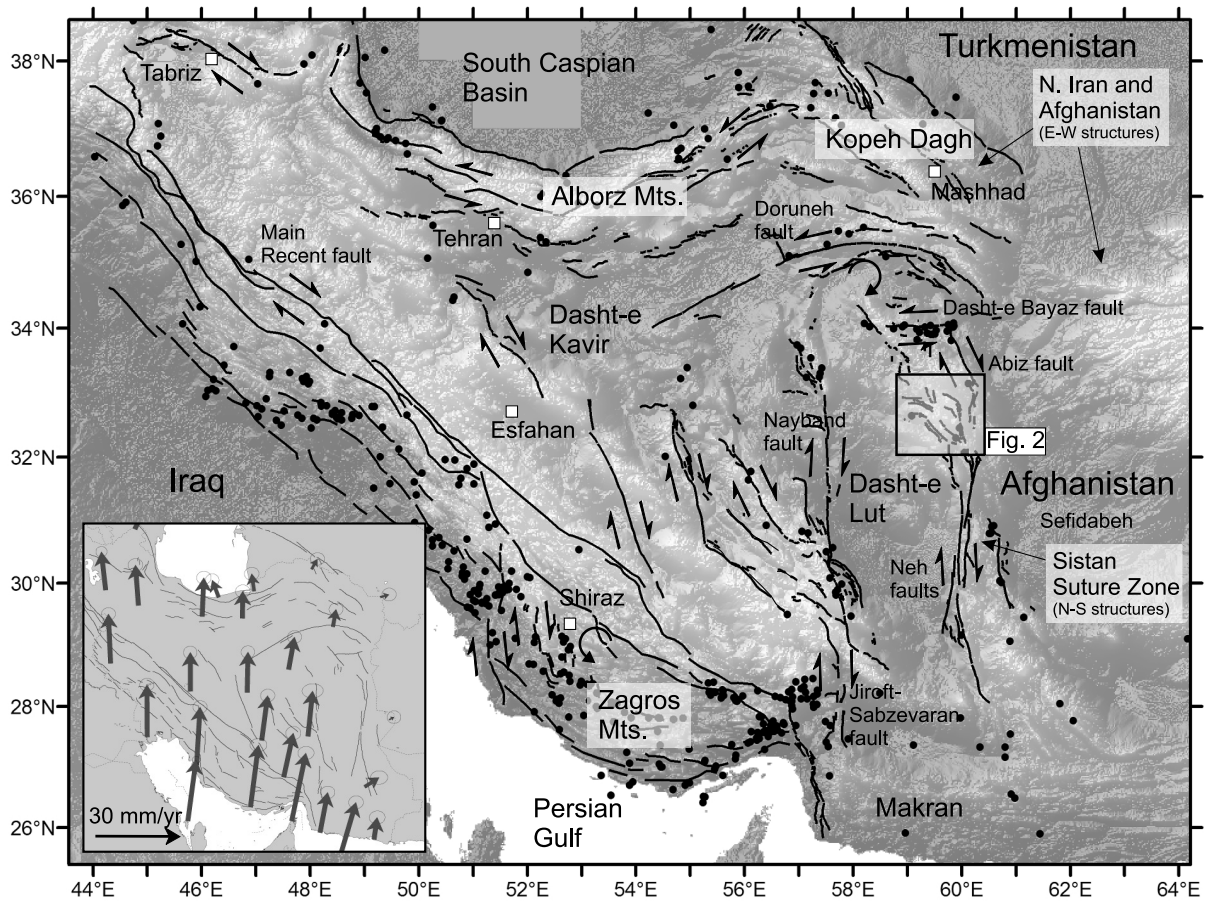

Figure 1. SRTM30 (Shuttle-borne Radar Topography Mission digital topography sampled at 30 arc sec pixel spacing [e.g., *Farr and Kobrick*, 2000]) topographic map of Iran showing active faults (drawn from observations of satellite imagery and digital topography), epicenters of earthquakes with $M_w > 5.3$ [from *Engdahl et al.*, 1998], major cities, and the location of other figures. The topography in eastern Iran and western Afghanistan shows the change from N-S orientation in the mountain ranges surrounding the Dasht-e lut to E-W orientation north of latitude ~32°N. The inset shows GPS velocities of points in Iran relative to stable Eurasia [from *Vernant et al.*, 2004] overlain on the fault map of *Berberian and Yeats* [1999]. Approximately 15 mm/yr of N-S right-lateral shear is accommodated between central Iran and Afghanistan. Both maps are in a Mercator projection.

Jackson, 1989]. Vertical axis fault rotation appears to be an important process in eastern Iran [e.g., *Jackson and McKenzie*, 1984; *Allen et al.*, 2006]. The aim of this paper is therefore to help us determine, through detailed mapping of the distribution of active faults, how relatively complicated tectonic configurations can be accommodated, aided by the preservation of subtle indications of active faulting in the arid and sparsely vegetated landscape of eastern Iran.

[7] We first describe and interpret the active faulting at Nauzad in the east of the study area (Figure 2). Faulting near Nauzad is known to have caused a large historical earthquake. We then extend our observations to search for active faulting in the region around Birjand (Figure 2). Historical earthquakes are known to have damaged Birjand, but have not been assigned with certainty to individual structures [e.g., *Ambraseys and Melville*, 1982; *Berberian and Yeats*, 1999]. Identifying the active faults is a useful first step in assessments of the seismic hazard to Birjand and nearby towns. We then use the distribution of active faults to make inferences on their likely role in the regional tectonics. In particular, we investigate how the faults at Birjand interact with one another to accommodate the overall regional strain in this part of Iran.

2. Active Tectonics of Iran

[8] The active deformation of Iran results from Arabia-Eurasia convergence. Shortening is accommodated by distributed faulting in high mountain ranges in the south (the Zagros) and the north (the Alborz and Kopeh Dagh) of the country (Figure 1). Surrounding regions to the north and east are aseismic and appear to be deforming at much lower rates [e.g., *Vernant et al.*, 2004]. The N-NNE motion of central parts of Iran relative to Afghanistan results in right-lateral shear of ~15 mm/yr in eastern Iran (Figure 1 inset) [*Vernant et al.*, 2004]. South of 34°N the N-S right-lateral

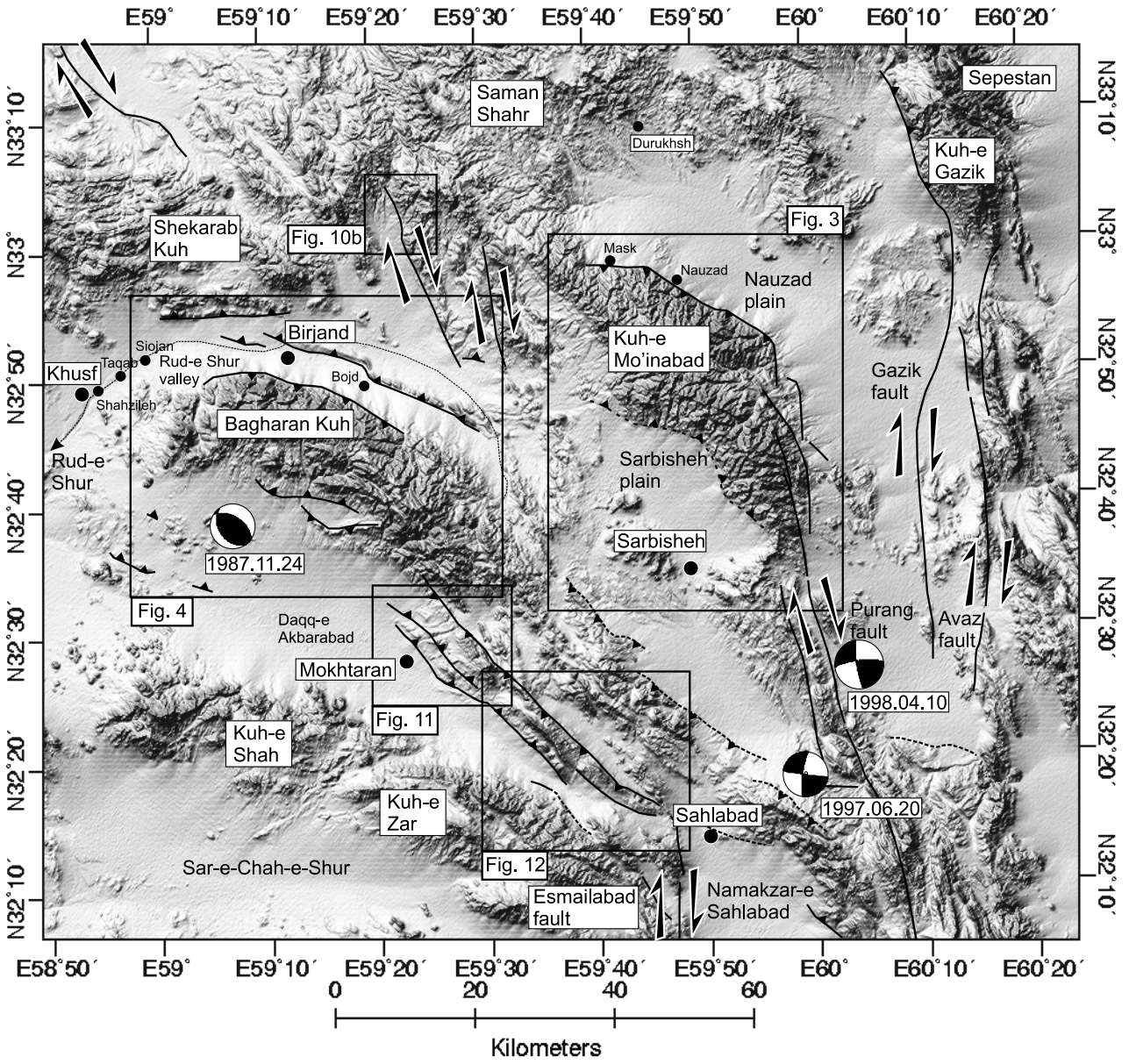

Figure 2. Shaded relief 90 m SRTM topography of the Birjand region showing major settlements, geographical regions, and fault zones (faults that we have not visited in the field, but which we suspect to be active, are marked as dashed lines). The fault plane solution of the 20 June 1997 earthquake is from *Berberian et al.* [1999]. The other two fault plane solutions are from the Harvard CMT catalogue. This, and all other maps, is in a local zone UTM projection.

shear is taken up on right-lateral strike-slip faults (e.g., Figure 1). North of 34°N left-lateral strike-slip faults are thought to take up the right-lateral shear by rotating clockwise [e.g., *Jackson and McKenzie*, 1984; *Walker et al.*, 2004; *Walker and Jackson*, 2004].

[9] In this paper, we are interested in how the transition between the N-S right-lateral faults and the E-W left-lateral faults in eastern Iran is accommodated by diffuse faulting around Birjand (e.g., Figures 1 and 2). No direct measurements of the rates of present-day deformation exist in our study area. We do however have Quaternary slip rate determinations on several of the N-S right-lateral faults bordering the Dasht-e Lut. *Regard et al.* [2005] estimate that the Jiroft-Sabzevaran fault system accommodates ~6 mm/yr of right-lateral slip across the southwestern Dasht-e Lut margin. Farther north, basalts displaced by the Nayband fault and dated at ~2 Ma [*Camp and Griffis*, 1982] imply that right-lateral slip rates across the western margin of the Dasht-e Lut have decreased to ~1.5 mm/yr [*Walker and Jackson*, 2002]. The remaining ~4 mm/yr of slip are presumably taken up across active faults within central Iran [e.g., *Vernant et al.*, 2004; *Walker and Jackson*, 2004]. A maximum of 6 mm/yr of

right-lateral shear west of the Dasht-e Lut implies that the remaining 8–9 mm/yr is accommodated to the east of the Dasht-e Lut, across the Sistan Suture Zone [*Vernant et al.*, 2004]. The strike-slip and thrust faults described in this paper are situated directly north of the east and west Neh faults, which are the most prominent right-lateral faults of the northern Sistan Suture Zone (e.g., Figure 1). A maximum of 8–9 mm/yr of total N-S right-lateral shear may therefore be accommodated on the active structures described in this paper.

3. Geology, Morphology, and Drainage

[10] Much of eastern Iran is occupied by desert depressions, with low elevations and high aridity (e.g., Figure 1). The Birjand region, by contrast, is relatively high, with a series of roughly NW-SE linear mountain ranges (Kuh-e Gazik, Kuh-e Mo'inabad, Shekarab Kuh, Bagharan Kuh, and Kuh-e Shah), reaching to elevations of over 3,000 m (Figure 2). The ranges are separated by narrow basins covered with alluvial deposits, and with typical elevations of 1500 to 1700 m. The geological map marks only the most recent alluvial cover as Quaternary in age. All older alluvial deposits and folded gravel beds are described as Neogene [*Eftekhar-Nezhad and Stocklin*, 1992]. A Neogene age of these deposits would suggest that the structures in which they are exposed are relics from the late Tertiary. However, the morphology of the folds (as described in section 5) and the available record of seismicity (section 4) show them to be active in the very recent past, and we are confident that the folded gravels are relatively young, and presumably date from the Quaternary.

[11] The mountain ranges expose Late Cretaceous to Eocene ophiolitic rocks of the Sistan Suture Zone, which are pervasively cut by inherited shear zones and faults [e.g., *Tirrul et al.*, 1983]. The trend of lithological units, and the major geological shear zones, run parallel to the topography. Therefore, in the south of the study area, the geological structures trend roughly N-S to NNW-SSE along the eastern margin of the Dasht-e Lut (Figure 1) [*Tirrul et al.*, 1983]. However, to the north of the study area, both the topography, and the geological structures, trend E-W (Figure 1) [*Jackson and McKenzie*, 1984]. The influence of the pre-existing structure on the distribution and orientation of active faults is discussed in section 6.2.

[12] Numerous short rivers arise within the parallel E-W mountain ranges of Qohestan and flow into the adjacent internally draining basins such as the Nauzad plain, Sarbisheh plain, Daqq-e-Akbarabad, Sar-e-Char-e-Shur, and Namakzar-e-Sahlabad (Figure 2). The only river to flow for any appreciable distance is the Rud-e Shur, which arises in the Bagharan Kuh mountains to the southeast of Birjand and flows westward through Birjand and Khusf to eventually drain into the Dasht-e Lut desert (Figure 2).

4. Recent and Historical Seismicity

[13] The city of Birjand has a long history as an important center of population [e.g., *LeStrange*, 1905; *Ambraseys and Melville*, 1977]. Although there have been many recent earthquakes in NE Iran (Figure 1), relatively few are located in the vicinity of Birjand (e.g., Figure 2). However, destructive earthquakes are known from the historical record. The only recorded earthquake attributed with certainty to an individual fault is the 1493 Nauzad earthquake (~50 km to the east of Birjand), which generated ~30 km of surface ruptures between the villages of Nauzad and Mask that were observed and described in a contemporary account [*Ambraseys and Melville*, 1977; *Berberian and Yeats*, 1999; *Berberian et al.*, 2000] (see also section 5.1).

[14] Up to three thousand people were killed and Birjand and surrounding villages (Shahzileh, Taqab, Siojan, and Bojd; see Figure 2) were destroyed by an earthquake in 1549 A.D. [e.g., *Ambraseys and Melville*, 1982; *Berberian and Yeats*, 2001]. No surface ruptures were reported following this earthquake. From the damage distribution the earthquake is likely to have occurred on a fault within the Rud-e Shur valley [*Berberian and Yeats*, 2001]. *Ambraseys and Melville* [1982] report the (earthquake induced?) destruction of Durukhsh village in the sparsely populated mountainous regions to the northwest of Nauzad in 1903 (Figure 2). *Berberian and Yeats* [2001] report a magnitude 5.2 earthquake (10 February 1940), with localized damage at Mokhtaran to the south of Birjand (Figure 2).

[15] Very few earthquakes have occurred in our study area during the modern instrumental age (Figure 2). Villages situated along the southern margin of the Bagharan Kuh mountain range were damaged by a M_w 5.3 earthquake on the 24 November 1987 [*Berberian and Yeats*, 1999]. The 1987 event was too small for the source parameters to be determined using long-period *P* and *SH* waveform modeling [e.g., *Berberian et al.*, 1999]. The Harvard centroid moment tensor (CMT) solution indicates an almost pure thrust mechanism. The moderate 20 June 1997 and 10 April 1998 earthquakes occurred close to the Purang strike-slip fault in the southeast of our study area (Figure 2). The fault plane solutions for both these events show either N-S right-lateral slip or E-W left-lateral slip.

[16] Instrumentally recorded large magnitude earthquakes have occurred both to the north and south of our study area. The M_w 7.2 Zirkuh event on the 10 May 1997 generated 125 km of surface ruptures along the NNW-SSE right-lateral Abiz fault (Figure 1). The 1997 Zirkuh event may be considered as part of the Dasht-e Bayaz earthquake sequence [*Berberian and Yeats*, 1999; *Walker et al.*, 2004], which has included three events of $M_w > 7$. To the south of the study area, a sequence of five thrust earthquakes (M_w 5.5–6.2) destroyed the village of Sefidabeh in February 1994 [*Berberian et al.*, 2000; *Parsons et al.*, 2006].

5. Active Faulting in the Birjand Area

[17] In this section, we present descriptions of late Quaternary movement on faults in the region around Birjand, many of which have not previously been described. As there have been few recent earthquakes in this area we cannot use seismology to constrain the nature and locations of faulting at depth. We therefore used satellite imagery and the SRTM (Shuttle-borne Radar Topography Mission [*Farr*

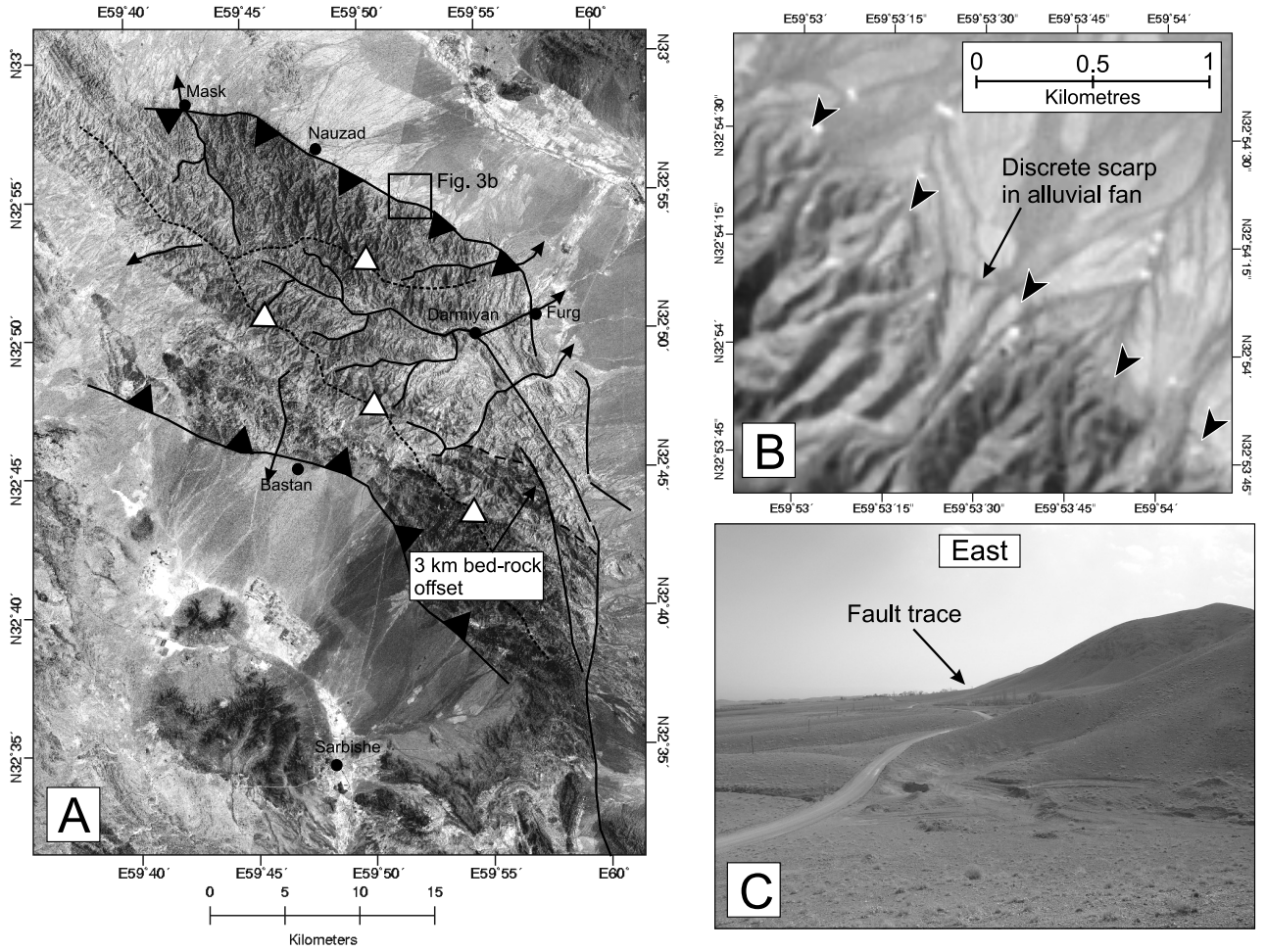

Figure 3. (a) Landsat TM+ satellite imagery (band 8) for the Kuh-e Mo'inabad region. Villages, mountain peaks, large rivers, and major faults are marked. The 1493 Nauzad earthquake produced ~30 km of ruptures along the northern margin of the mountains between Mask and Furg. (b) ASTER satellite imagery of the Nauzad fault scarp. The fault follows the margin of the Kuh-e Mo'inabad mountains but forms a discrete step in alluvial fan deposits where it crosses river valleys. (c) The Nauzad fault in the field (looking east from 32°58′09.8″N, 59°43′28.4″E). The fault follows the base of the mountains.

and Kobrick, 2000]) digital topography data set to locate indicative signs of active faulting in the landscape, using similar styles of observation to those by *Walker et al.* [2003] and *Walker* [2006]. Our remote sensing observations are complemented by field observations in March 2004.

5.1. Kuh-e Mo'inabad

[18] The 1493 Nauzad earthquake produced ~30 km of surface ruptures along the northern margin of the Kuh-e Mo'inabad mountains (see Figure 3) [e.g., *Ambraseys and Melville*, 1977; *Ambraseys and Melville*, 1982; *Berberian and Yeats*, 1999]. The reported earthquake ruptures lie along the clear trace of a thrust fault, which can be traced both in satellite imagery and in the field (e.g., Figure 3). The fault forms a sharp topographic break at the base of the Mo'inabad mountains, and forms discrete scarps in alluvial deposits where northward flowing rivers exit the Mo'inabad mountains (e.g., Figure 3b). The southern margin of the Mo'inabad mountains near the village of Bastan is also very sharp. We have marked this fault on our map but have not visited this area in the field to check for Late Quaternary movements. Both the Nauzad fault and the suspected fault at Bastan are parallel to the strike of lithological units within Kuh-e Mo'inabad, which trend NW-SE [*Eftekhar-Nezhad and Stocklin*, 1992] (e.g., Figure 3a).

[19] The Nauzad thrust fault links at its eastern end with the N-S right-lateral Purang fault [*Berberian et al.*, 2000]. In detail, the northern end of the Purang fault appears to break into at least three strands, which curve round to the east and end within the Mo'inabad mountains. The easternmost strand displaces bedrock by at least 3 km (Figure 3a).

5.2. Southern Rud-e Shur Valley: Bagharan Kuh Range Front

[20] The Bagharan Kuh range front appears as a very sharp line in SRTM topography, and separates Tertiary

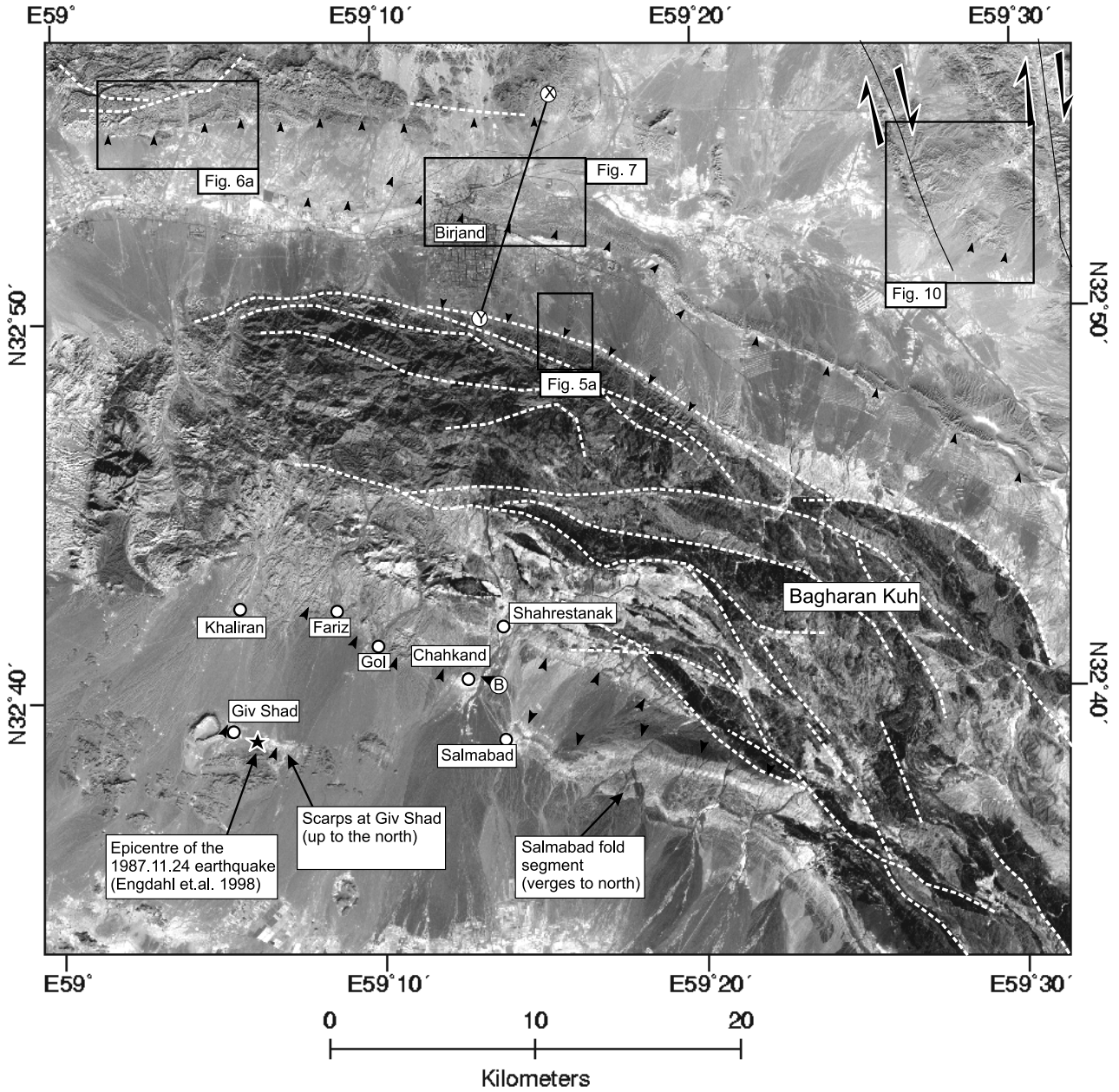

Figure 4. (a) ASTER satellite image (band 3n) of Birjand, Bagharan Kuh, and surrounding basins. Black arrows point to thrust faults. The Shekarab Kuh range front can be seen along the northern margin. Anticlinal folding (the Giv fold system) occurs along the southern Bagharan Kuh range front. Folding in alluvial gravels at Chahkand verges to the south. The prominent E-W trending anticline running eastward from Salmabad appears to verge northward. The two folds may be underlain by opposing thrust faults. Small southward facing E-W scarps occur near Giv Shad and also farther west (see Figure 2). Major geological faults (marked by dashed white lines) within the mountains are parallel to the trend of the topography and also the trend of the active faults. Boxes mark the location of Figures 5a, 6a, 7, and 10. The line of section in Figure 9 is marked X-Y.

ophiolitic rocks to the south from the Quaternary alluvial cover in the Rud-e Shur valley to the north [*Eftekhar-Nezhad and Stocklin*, 1992] (Figures 4 and 5). The range front roughly follows a shear zone within ophiolitic material (e.g., Figure 4), which is clearly identified in the field from a distinctive light brown hydrothermal listvinite alteration. The range front therefore appears to follow structural weaknesses inherited from the time of emplacement of the ophiolites, which is thought to be between ~89 Ma and 34 Ma [e.g., *Tirrul et al.*, 1983].

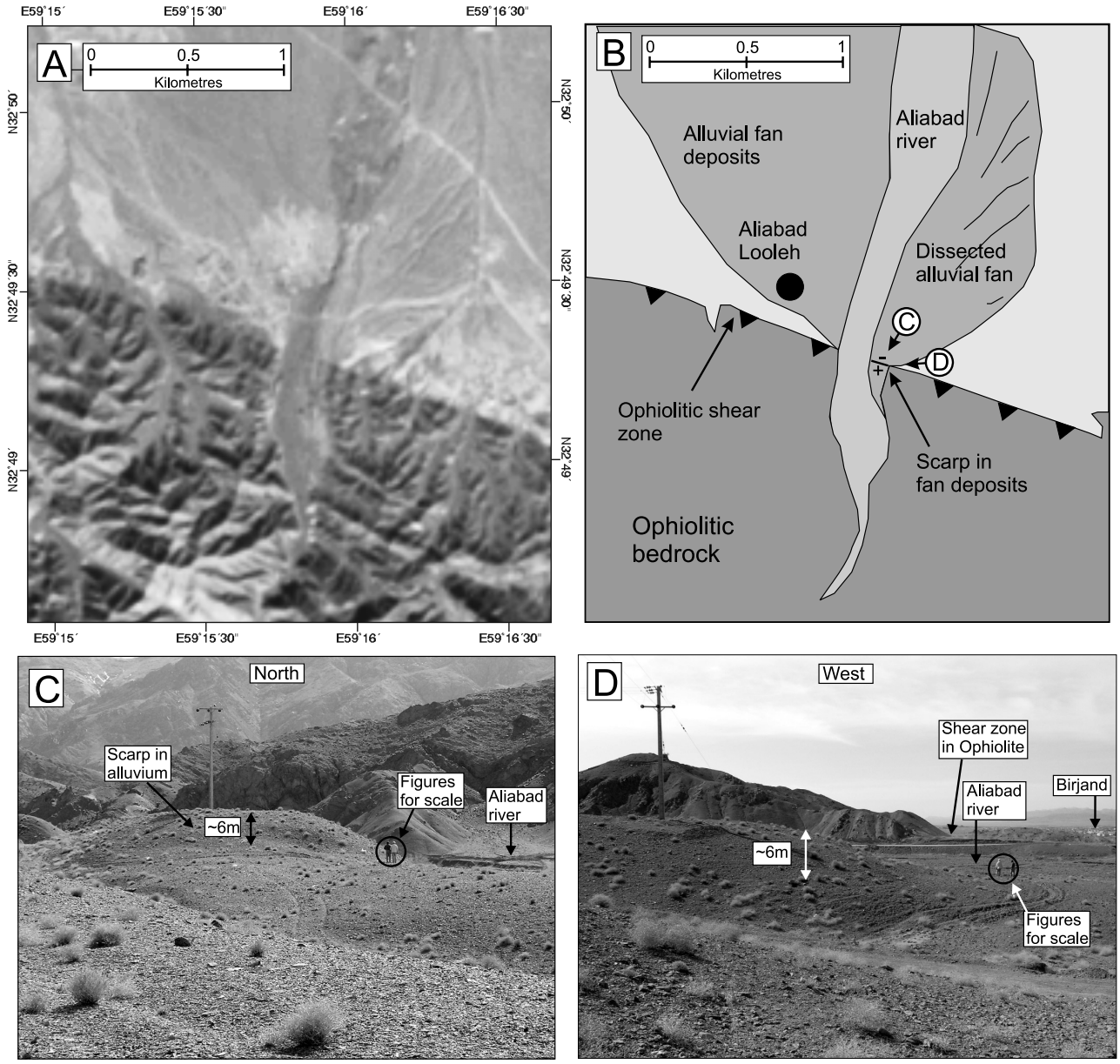

Figure 5. (a) ASTER satellite image (band 3n) of the Bagharan Kuh mountain range front to the south of Birjand (see Figure 4 for location). Aliabad-Looleh village is situated on the western bank of a northward flowing river, which exits the Bagharan Kuh mountains in a channel incised through bedrock and alluvial deposits. The main underground canal (Qanat) water source for Birjand originates here. The river has cut through at least one alluvial surface. An ~6 m high scarp is seen in the top surface of the incised alluvium at the range front. (b) Sketch of Figure 5a showing the major bedrock and Quaternary features. (c) View south from 32°49′20.8″N, 59°16′05.4″E of the ~6 m high scarp in alluvial material at the Bagharan Kuh range front. (d) View west along the Bagharan Kuh range front scarp. At the western side of the river the range front follows an altered shear zone in ophiolitic rocks. The city of Birjand is seen in the distance.

[21] For much of its length, the Bagharan Kuh range front fault does not cut through alluvial deposits, and slip related to the most recent (Plio-Quaternary) period of faulting cannot be confirmed. We found one location (initially identified from aerial photographs) where the range front fault does displace alluvial cover at the village of Aliabad-Looleh to the south of Birjand (Figure 5). At this location, a northward flowing river has incised through an alluvial gravel fan deposited as the river exits the mountains. A thin (~20 m wide) remnant of the old fan is preserved on

the eastern side of the river cutting (Figures 5a and 5b). The top surface of the fan remnant is displaced vertically by ~6 m at the range front (Figures 5c and 5d). The scarp in alluvium is directly along line with outcrops of hydrothermally altered material within a shear zone (Figure 5d). The Bagharan Kuh range front fault does therefore appear to be active in the late Quaternary.

5.3. Northern Rud-e Shur Valley: Shekarab Kuh Range Front

[22] The Shekarab Kuh mountain ranges form the northern border of the Rud-e Shur river valley (Figure 6). Eroded scarps in alluvium are observed in the field (e.g., Figures 6b and 6c) where three terrace levels have been incised and abandoned by down cutting of the southward flowing river. The lower two terraces are now ~2 m and ~5 m above the present-day river level (Figure 6c). Similarly incised terrace remnants can be seen within the mountain ranges in ASTER imagery (Figure 6a). In Figure 6c, the incised terrace remnants appear to be truncated along a sharply defined E-W scarp, with possible roll-over of cemented layers within the terrace material. Clearer evidence of folding of terrace material at the fault trace was found at 32°55′10.0″N, 59°06′09.7″E, where gravels are tilted ~10° to the south over a distance of ~5 m (Figure 6d). Ophiolitic rocks within Shekarab Kuh trend E-W (e.g., Figure 6a), and are cut through by numerous geological faults [*Eftekhar-Nezhad and Stocklin*, 1992]. The active range front fault appears to follow this inherited E-W trend.

5.4. North Birjand Fault: Anticlinal Folding at Birjand

[23] The north Birjand anticlines are shown in Figures 4 and 7. The main fold segment is ~35 km long, ~2 km wide and is developed in alluvial gravels shed from the surrounding mountain ranges. A shorter (~3–4 km long) fold segment is developed to the northwest of Birjand. Birjand town is built within a wide fluvially incised gorge within the main fold segment (Figure 7). The fold is flat topped (Figure 7) but both the north and south facing flanks form sharp, linear scarps (e.g., Figures 7 and 8c). The overall vergence is to the south, with an axis that is close to the southern margin of the fold. Bedding exposed in the southern fold margin shows rapid steepening of beds over distances of only ~100 m (e.g., Figure 8a). Beds close to the southern margin have dips of up to 75°S (Figures 8a and 8d). Minor faulting is seen in several locations. Close to the fold axis, steeply dipping normal faults are observed. The E-W trending normal faults dip both to the north and south, and typically have displacements of ~10 cm (Figure 8b). Southward dipping thrust faults with displacements of several meters cut through the northern fold limb in several locations (e.g., Figure 8e), including very close to the fold axis (Figure 8f).

[24] Topographic profiles across the fold show the region north of the fold is elevated with respect to the area south of the fold (Figure 9a). This height change may result from uplift above a northward dipping fault at depth, as seen elsewhere in Iran [e.g., *Berberian*, 1979; *Walker et al.*, 2003]. Movements on blind thrust faults cause deformation of the Earth's surface in the form of anticlinal folding [e.g., *Stein and King*, 1984; *Stein and Yeats*, 1989], which may in turn be accommodated by a whole range of secondary faults [e.g., *Philip and Meghraoui*, 1983; *Philip et al.*, 1992; *Bayasgalan et al.*, 1999b; *Berberian*, 1979; *Oskin et al.*, 2000; *Walker and Jackson*, 2002], including many of the features seen at Birjand (as shown in Figure 9b). The flat top and steep scarps on both the northern and southern flanks of the fold suggest that each limb is underlain at reasonably shallow depths by thrust faults of opposing dip, as in the sketch in Figure 9b. The overall southward vergence and hanging wall uplift to the north suggest that the fault under the southern limb is dominant.

5.5. Strike-Slip Faulting at Shahlabad

[25] A number of N-S trending faults displace bedrock right-laterally within the mountains northwest of Nauzad (Figure 2). The village of Shahlabad is situated on the westernmost of these faults (Figure 10). Activity on the Shahlabad fault is inferred from the displacement of alluvium (marked as Neogene on the geological map [*Eftekhar-Nezhad and Stocklin*, 1992], but likely to be from the late Quaternary, see section 3) along the fault trace, which can be seen in ASTER satellite imagery (e.g., Figures 10a and 10b).

[26] We visited the southern end of the fault at Shahlabad in March 2004. The village is built on the fault scarp (Figure 10d), which is at least 10 m high and faces westward. Uplifted river gravels are exposed in a river cutting north of Shahlabad near 32°51′54.3″N, 59°27′29.3″E (Figure 10e). The uplifted gravels are folded over a distance of ~500 m with a westward dip at the scarp, and an eastward dip in the east (Figure 10f). Terracing in the sides of the river cutting (Figure 10e) indicates a lowering of the river level with respect to the eastern side of the fault, presumably caused by uplift at the fault. Minor E-W folding in alluvium is observed running east from Shahlabad (Figures 10a, 10c, and 10f). In contrast to the other active faults mapped around Birjand, the strike-slip faulting at Shahlabad does not appear to show a close relationship with the older geological structure.

5.6. Folding and Faulting South of the Bagharan Kuh Mountains

[27] Satellite imagery and digital topography show a system of folds along the southern margin of Bagharan Kuh, from Sahlabad in the east toward Khusf in the west (Figure 2). We call these structures the Giv fold system. The strike of the Giv folds follow the overall orientation of Bagharan Kuh, and the strike of geological structures within the mountains, with NW-SE fold axes in the eastern parts of the system, and roughly E-W axes in the west [*Eftekhar-Nezhad and Stocklin*, 1992] (Figure 2).

[28] The western parts of the Giv fold system are shown in Figure 4. The villages of Gol, Fariz, Kariz Now, Chahkand, Khaliran, Ghasabeh, Shahrestanak, and Salmabad were damaged by an earthquake on the 24 November 1987 [*Berberian and Yeats*, 1999; *Jackson*, 2001] (also see section 4), with the greatest damage at Gol. Southward

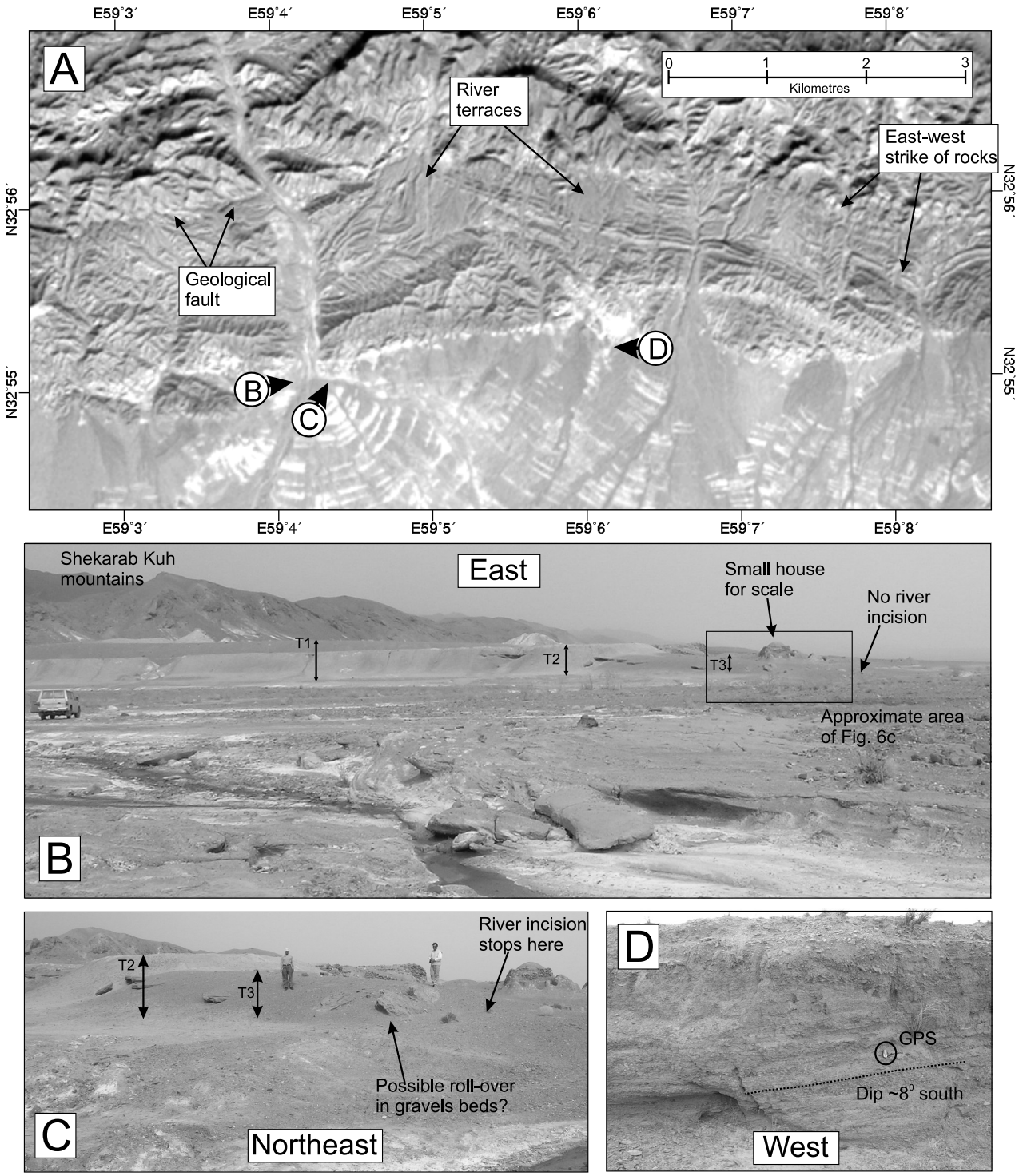

Figure 6. ASTER satellite image (band 3n) of the Shekarab Kuh mountain range front to the north of Birjand (see Figure 4 for location). Note how abandoned river terraces present within the mountains stop abruptly at the range front. Geological units north of the range front strike parallel to the E-W active fault. Geological faults within the mountains are also oriented E-W. (b) View looking east from 32°55′01.5″N, 59°04′23.7″E at the Shekarab Kuh range front. Three abandoned river terrace levels end at the range front. (c) View east from 32°55′01.7″N, 59°04′28.4″E of the river terraces shown in Figure 6b (figures for scale). (d) View looking west at gravels exposed in a stream cutting at 32°55′10.0″N, 59°06′09.7″E. The gravels dip ~8° to the south (GPS for scale).

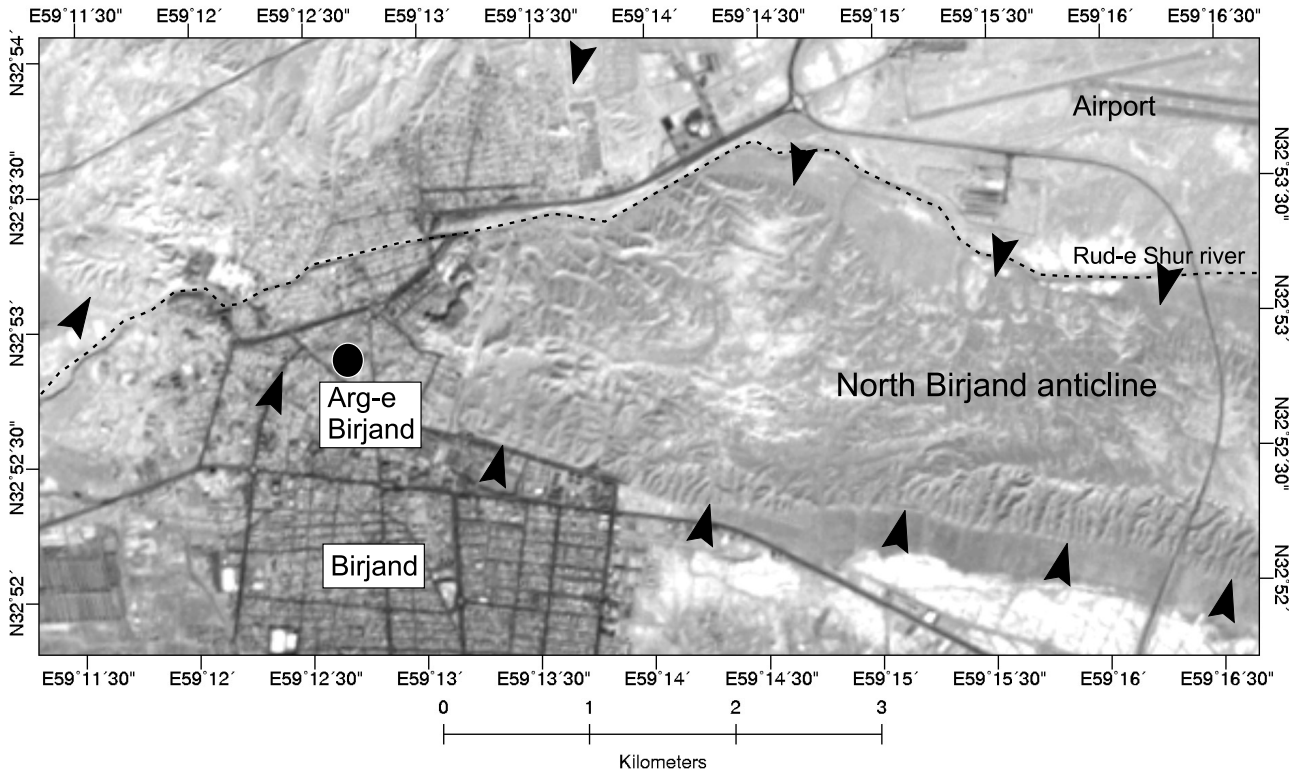

Figure 7. ASTER image of Birjand town (see Figure 4 for location). The old part of Birjand city is built within the gorge of the Rud-e Shur river as it cuts through a ~2 km wide E-W trending anticline. The Arg-e Birjand (the old fortress of Birjand) is positioned on an isolated hill, composed of uplifted and folded alluvium, which overlooks the bazaar district. Newer parts of the city extend southward across the alluvial apron toward the Bagharan Kuh range front (e.g., Figure 4).

verging uplifted and folded gravel beds are exposed in a river cutting near the village of Chahkand (Figure 4). The fold axis is at 32°40′32.7″N, 59°12′59.7″E. Minor dip-slip faulting, following a small topographic saddle, with displacements of ~1–2 m, were observed at the fold axis.

[29] Discontinuous scarps with a line of springs are observed at Giv (Figure 4). We found further short scarps (less than ~5 km in length) to the west of Figure 4. These scarps are marked with thrust fault symbols on Figure 2. Another fold segment runs eastward from the village of Salmabad in Figure 4. This fold segment is at least 15 km long and ~5 km wide. Folded gravels overlie outcrops of volcanic rocks in the core of the anticline. Dips in folded gravels within the Salmabad fold segment, and the location of the axis close to the northern margin of the fold, appear to indicate a northward vergence.

[30] Close to the village of Mokhtaran (Figure 11), the folds trend NW-SE, along the margin of Bagharan Kuh (seen in the top right corner of Figure 11). Folding is confined to a region of uplift ~8 km wide, in which remnants of folded and incised gravel beds (of presumed late Quaternary age, see section 2) lie on older (Neogene) marl beds, with occasional tuff layers, which are exposed along the southwestern and northeastern margins of the zone of uplift [*Eftekhar-Nezhad and Stocklin*, 1992](Figure 11b). A prominent synclinal axis runs through the center of the uplift. Subparallel anticline axes are identified close to the southwestern margin of the uplift (Figure 11). Marls are exposed in the cores of the folds. The marls are exposed right up to the northeastern margin of the uplift. These observations suggest that the presumably southward dipping fault underlying the northeastern margin of the uplift reaches to the surface as a thrust, but that slip on the opposing northward dipping thrusts under the southwestern margin is taken up, at least partly, by folding at the surface.

[31] Further east, the zone of uplift (now called Kuh-e Bazu), narrows to ~5 km width (Figure 12). Relief across Kuh-e Bazu reaches 200 m (Figure 12c). Sharp breaks in slope, abrupt limits to incision, and clear scarps in alluvium are observed in satellite imagery and digital topography along both margins of the uplift (Figure 12). Beds exposed in Kuh-e Bazu strike NW-SE and dip up to 30°NE across the entire zone of uplift [*Eftekhar-Nezhad and Stocklin*, 1992]. The topography is also steeper in the southern margin of Kuh-e Bazu, suggesting that the northward dipping thrust under the southwestern margin of the uplift is the dominant structure. The Kuh-e Bazu uplift continues eastward to longitude ~59°48′E (Figure 12a), where the topography stops abruptly at the northern end of the Esmailabad right-lateral strike-slip fault (Figure 12a). We cannot demonstrate a definite link between the strike-slip and thrust faults as we can at Nauzad (section 5.1).

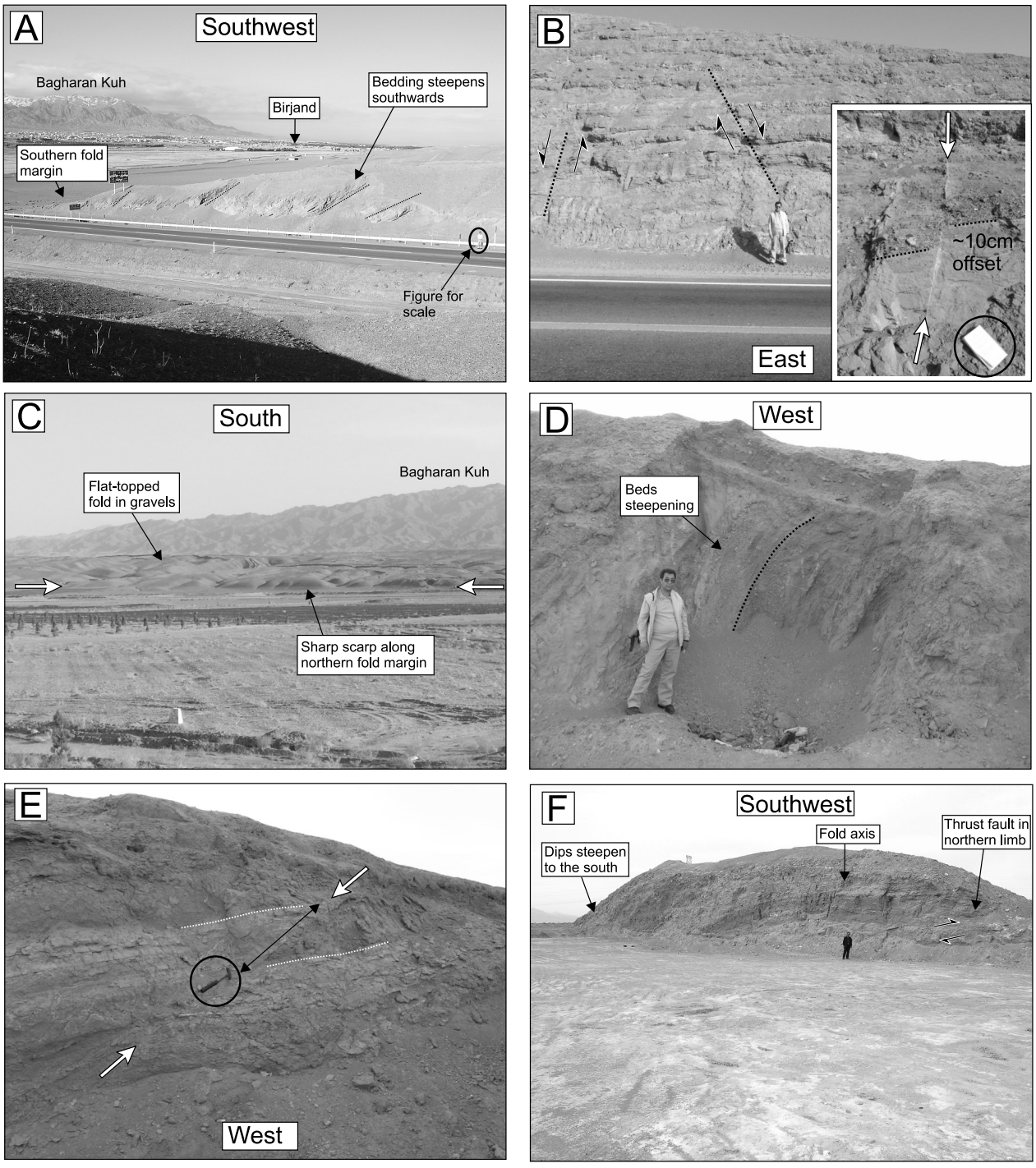

Figure 8. Photographs of the north Birjand anticline. (a) View northwest from 32°52′05.4″N, 59°16′28.4″E of the southern margin of the north Birjand anticline. Gravels exposed in the road cutting increase in dip toward the southern fold margin (from ~75°S to ~45°S over a distance of 50 m). (b) View east of normal faulting exposed in a road cutting at 32°52′13.5″N, 59°16′32.9″E. The inset shows a 10 cm offset in gravel beds (across the left-hand fault in the main photograph).(c) View south at the northern margin of the north Birjand anticline (taken from 32°53′33.7″N, 59°15′54.2″E. (d) View west of gravels beds exposed in the southern limb of the north Birjand anticline at 32°52′37.9″N, 59°13′17.6″E. The beds steepen from ~30°S to ~65°S across the photo. (e) View west of a secondary thrust fault (dip ~30°S, displacement ~50 cm, hammer for scale) cutting the northern limb of the north Birjand fold at 32°52′43.6″N, 59°13′15.4″E. (f) Exposure of the anticline axis at 32°53′19.2″N, 59°12′02.7″E. The northern limb is much steeper than the southern limb and is cut by a thrust fault.

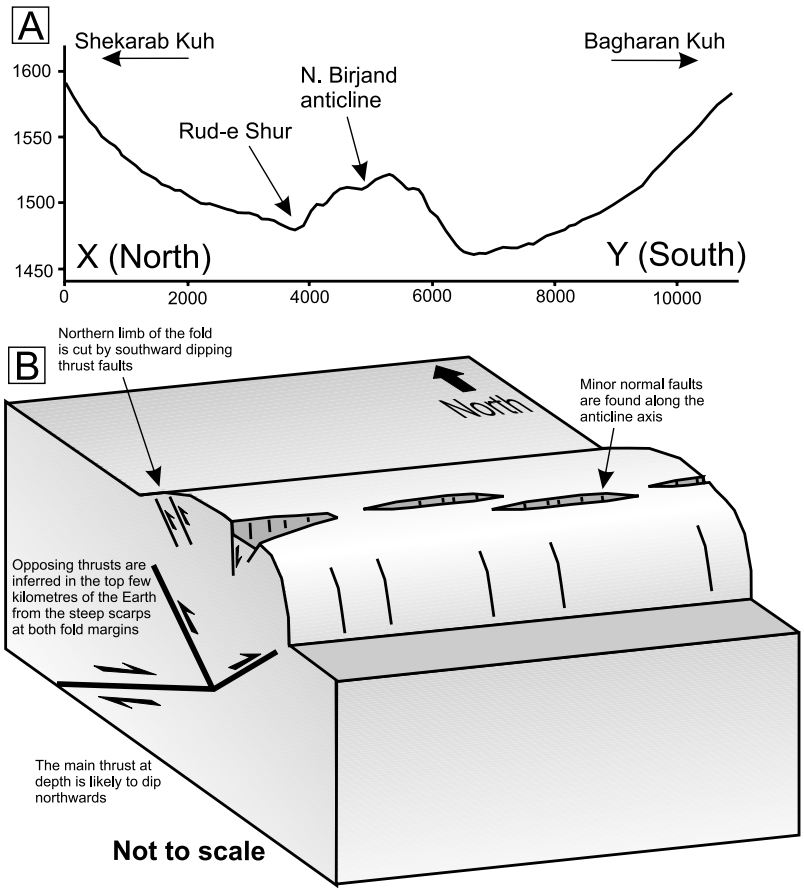

Figure 9. (a) Profile through SRTM topography along the line X-Y in Figure 4. Relief across the north Birjand anticline is ~50 m, much less than the 100–150 m of relief across the alluvial fans both to the north and the south. The fold is relatively flat on top, with steep scarps on both margins. (b) Sketch of structures observed in the north Birjand anticline and interpretation of the faulting at depth. The overall vergence is to the south, with both the fold axis and the steepest dips in gravel beds observed close to the southern fold margin. These observations imply a northward dipping fault beneath the anticline. The relatively flat top and the steep scarps preserved on both fold margins indicate that the fold is underlain at relatively shallow depths (probably the top 2 km of the Earth) by opposing north and south dipping thrusts. Fold growth is accommodated by secondary normal faulting close to the fold axis and southward dipping secondary thrust faults cutting the northern fold limb.

However, the abrupt end of the Giv fold system at the Esmailabad fault, and the absence of indications of active strike-slip faulting to the north of the Giv folds within the heavily sheared bedrock of the Bagharan Kuh mountains [*Eftekhar-Nezhad and Stocklin*, 1992], suggest to us that the Esmailabad and Giv fault systems are linked, and join at ~32°16′N, 59°48′E (Figure 12a).

5.7. Active Faulting Around Birjand: A Summary

[32] In the above descriptions we have found indications of widespread active faulting both along the range fronts and within the basins of the Birjand region (e.g., Figure 2). It is likely that we have not located all of the active faults. This is especially true in the mountainous regions such as Saman Shahr and Shekarab Kuh to the north (Figure 2), where there are few young alluvial deposits to guide us toward the youngest faults. Nevertheless, the active faults shown in Figure 2 are the best available guide we have at present. In section 6, we discuss the implications of our observations for the regional tectonics.

6. Discussion

[33] In section 5 we have produced a map of active faulting in the Birjand region. In the following discussion we use this map to first describe how regional strain may be accommodated by active faulting in this part of Iran. In section 6.1, a simple kinematic model is produced to explain how the mixture of N-S and E-W faults might accommodate the regional N-S right-lateral shear. In section 6.2, we discuss the influence of preexisting structural weaknesses in determining the pattern of active faulting.

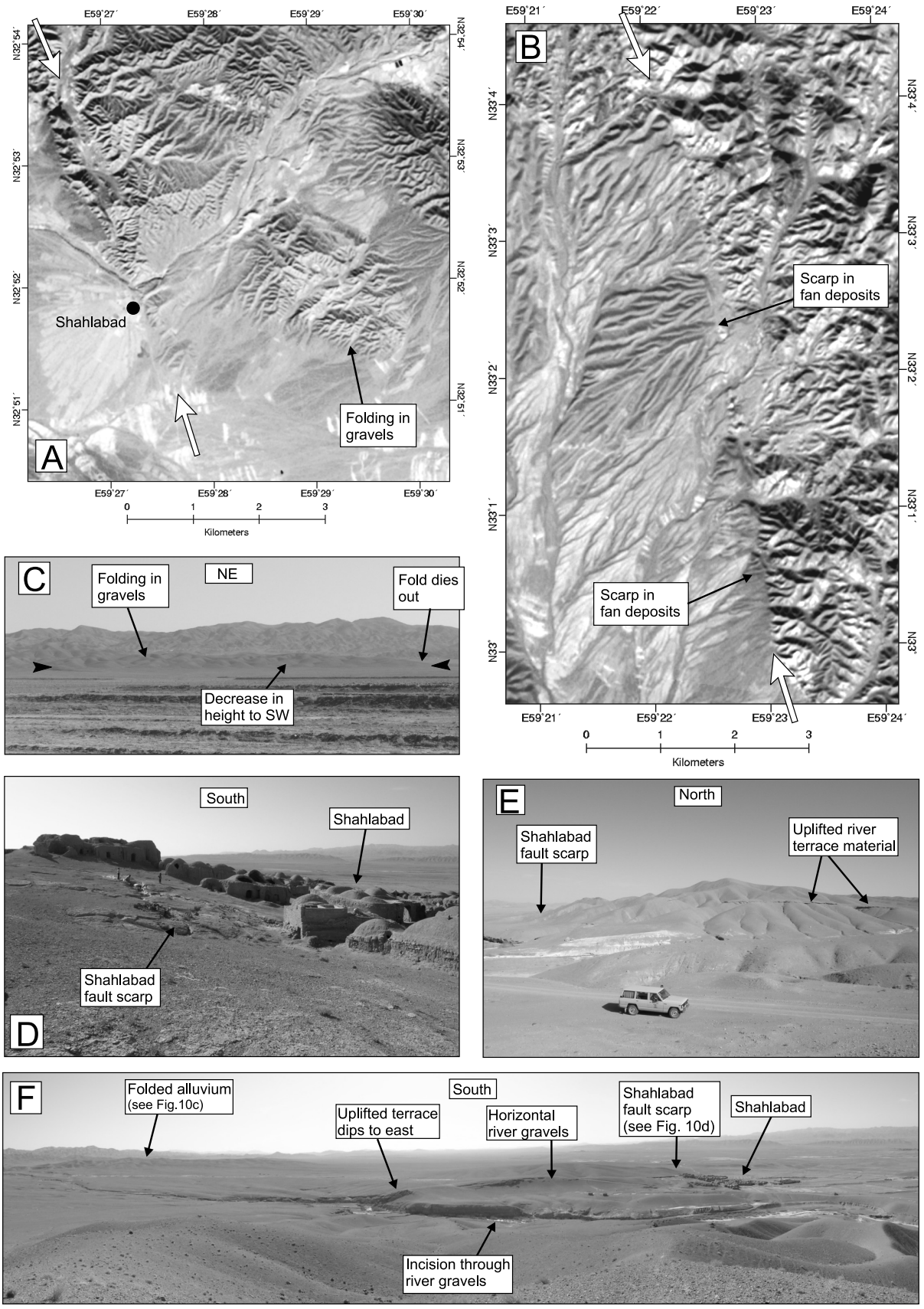
A
Shahlabad
Folding in gravels
E59°27′
E59°28′
E59°29′
E59°30′
N32°54′
N32°53′
N32°52′
N32°51′
0 1 2 3
Kilometers
B
Scarp in fan deposits
Scarp in fan deposits
E59°21′
E59°22′
E59°23′
E59°24′
N33°4′
N33°3′
N33°2′
N33°1′
N33°
C
Folding in gravels
NE
Fold dies out
Decrease in height to SW
D
South
Shahlabad
Shahlabad fault scarp
E
North
Shahlabad fault scarp
Uplifted river terrace material
F
Folded alluvium (see Fig.10c)
South
Uplifted terrace dips to east
Horizontal river gravels
Shahlabad fault scarp (see Fig. 10d)
Shahlabad
Incision through river gravels

Figure 10

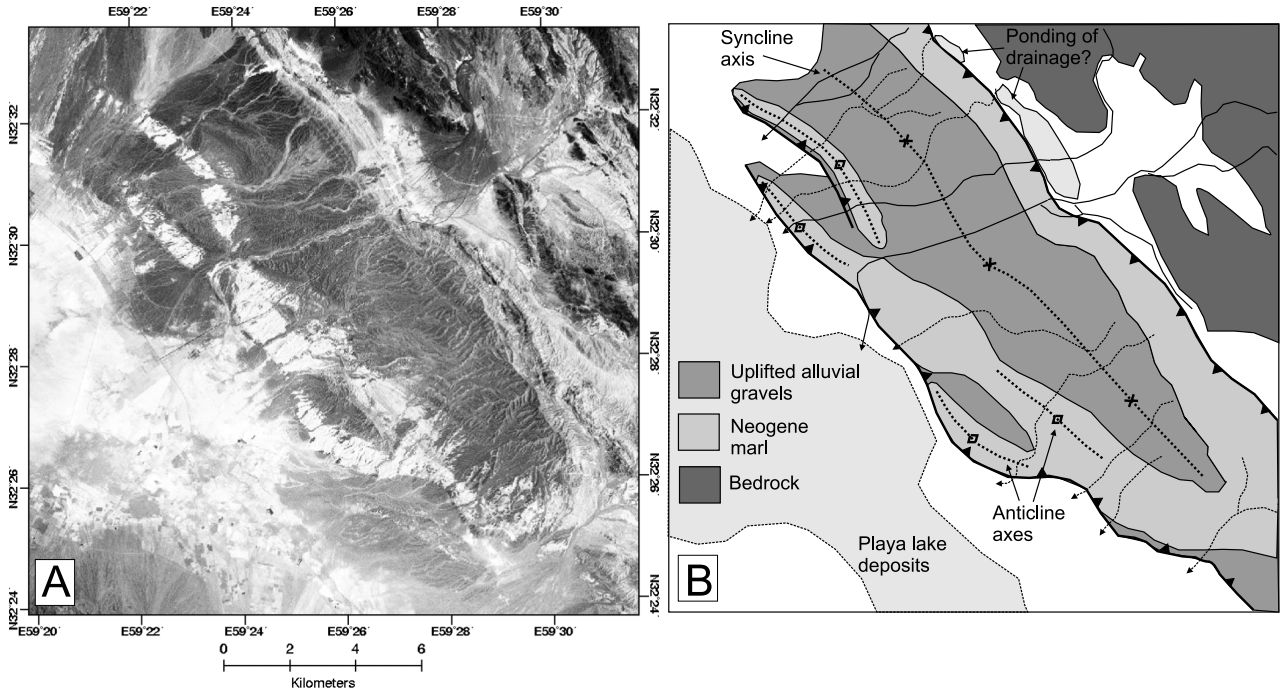

Figure 11. (a) ASTER satellite image faulting and folding near the village of Mokhtaran (see Figure 2 for location). A NW-SE trending zone of uplift ~8 km wide exposes Neogene marls at both margins. The marls are overlain by alluvial gravels, which are incised by southward flowing drainage. (b) Sketch of the same region, showing the distribution of exposed sediments within the folded region, and the major drainage systems. Active river systems are marked as black lines. Abandoned river systems are marked as dashed lines.

6.1. Accommodation of Strain in NE Iran

[34] In numerous examples around the world, active strike-slip faults appear to end in dip-slip faults, with displacements that die away from the junction between the two [e.g., *Bayasgalan et al.*, 1999a; *Berberian et al.*, 1999, 2000; *Meyer et al.*, 1998; *Parsons et al.*, 2006]. The Nauzad thrust along the northern margin of Kuh-e Mo'inabad is an example of this type of structure with the thrust linking at its eastern end to the Purang strike-slip fault [see *Berberian et al.*, 2000, Figure 14].

[35] At first glance, the E-W thrust faults along the Rud-e Shur valley appear to have a similar role to the thrusts at Nauzad, forming the northern termination of the Esmailabad strike-slip fault (Figure 2). On closer inspection, however, the Esmailabad strike-slip fault does not appear to reach any farther north than latitude ~32°15′N, where it apparently joins with the Giv fold system at Sahlabad (Figures 2 and 12). The strike-slip fault trace is not seen in alluvial deposits to the north of the junction, and well exposed NW-SE trending ophiolitic bedrock within the Bagharan Kuh mountains, although heavily deformed, does not appear to be displaced by throughgoing strike-slip faulting (see section 5.6). The Giv folds appear to be more highly developed in the eastern parts (Figures 11 and 12) than in the west, where only small, discontinuous scarps are observed (Figure 4). A westward decrease in slip would be compatible with the observations of *Bayasgalan et al.* [1999a].

[36] *Bayasgalan et al.* [1999a] suggest that structures like those seen at Nauzad and Giv may arise as a consequence of spatial variations in style of faulting. For instance thrust faults that link to the end of strike-slip faults, and whose displacement dies away from the junction between the faults, can allow transition between fault configurations that require vertical axis rotation, and fault configurations that require no vertical axis rotation, while still achieving the overall regional deformation. The termination of the Esmailabad and Purang strike-slip faults in the Giv and Nauzad thrust systems may thus allow the style of faulting to change

Figure 10. (a) ASTER satellite image (band 3n) of the region around Shahlabad village (see Figure 2 for location). The village is situated on a small scarp (~10 m high) that runs NNW from the village (the Shahlabad fault). Southeast of the village, a region of folded river gravels is observed. (b) ASTER image of the Shalabad fault scarp ~20 km north of Shahlabad village. The fault has cut through and beheaded a series of alluvial fans. (c) View northeast from 32°50′34.8″N, 59°27′46.9″E of anticlinal folding in gravels to the east of Shahlabad village. (d) View south from 32°51′54.3″N, 59°27′29.3″E of west facing fault scarp at Shahlabad village. (e) View north from 32°51′54.3″N, 59°27′29.3″E. Westward flowing streams incise to the east of the scarp. (f) View southward from 32°52′09.7″N, 59°27′28.4″E along the uplifted (eastern) side of the Shahlabad fault. Streams incise through uplifted and folded gravel beds. The fold is ~500 m wide. Further folding in gravels is seen in the far east (left) of the image.

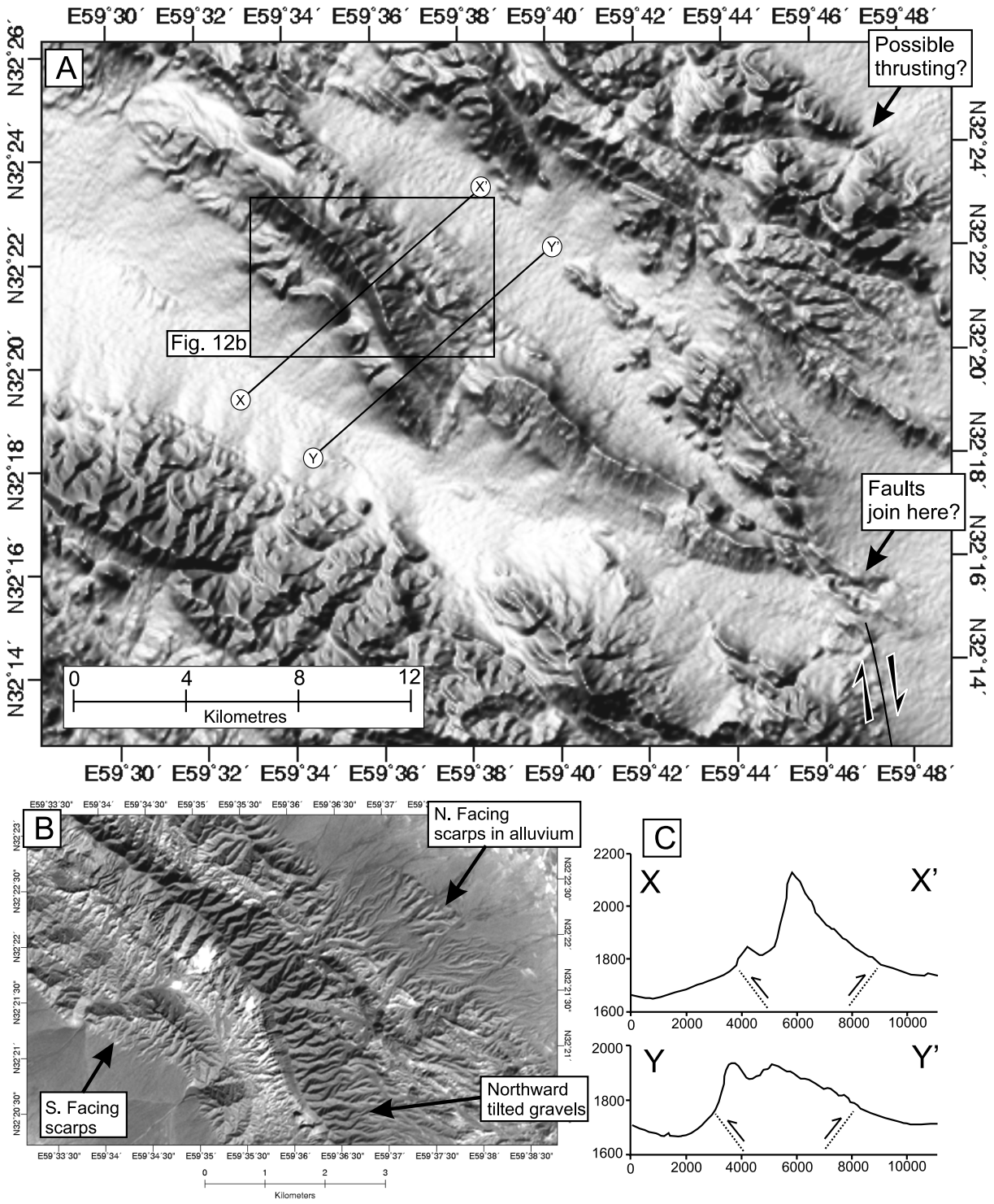

Figure 12. (a) SRTM topography of folding and faulting at Kuh-e Bazu at the southeastern end of the Giv fold system (see Figure 2 for location). The Esmailabad right-lateral strike-slip fault is seen in the bottom right of the image. The trace of the Esmailabad fault ends at Kuh-e Bazu and may suggest that the two structures are linked. (b) ASTER satellite image of part of Kuh-e Bazu. Scarps in alluvial material are developed at both margins of the uplift, but the structure has an overall vergence to the south. (c) Profiles taken through SRTM topography along the lines of section in Figure 12a. The profiles show the asymmetry of the uplift with the highest topography and steepest slopes close to the southwestern margin. Opposing thrust faults are inferred from the scarps observed in the ASTER imagery.

from one dominated by N-S right-lateral faulting in the south, to the diffuse E-W thrusting observed in the north of the study region (Figure 13).

[37] The northward transition from N-S strike slip to diffuse thrusting probably results from the more regional change to E-W left-lateral faulting farther north. The accommodation of N-S right-lateral shear on E-W left-lateral structures requires clockwise vertical axis rotation [e.g., *Jackson and McKenzie*, 1984], which in turn results either in shortening across the strike-slip faults themselves, or in diffuse deformation of intervening crustal material [e.g., *McKenzie and Jackson*, 1983; *Bayasgalan et al.*, 1999a; *Berberian et al.*, 2000]. Diffuse faulting is observed farther north in the alluvial plains surrounding the Dasht-e Bayaz fault [e.g., *Berberian*, 1976; *Walker et al.*, 2004]. A number of the faults around Dasht-e Bayaz have generated destructive earthquakes [e.g., *Berberian and Yeats*, 1999; *Walker et al.*, 2004]. The widespread active faulting observed within our study area probably marks the southern limit of this diffuse deformation zone. It is almost certain that further seismogenic faults exist north of our study area within the volcanic highlands of Shekarab Kuh and Saman Shahr. Numerous enclosed basins, sharp linear breaks in topography, and widespread river downcutting within Saman Shahr point toward the presence of active faults. Because of an absence of clearly displaced Quaternary features in satellite imagery a detailed map of active faulting within Shekarab Kuh and Saman Shahr would require extensive fieldwork.

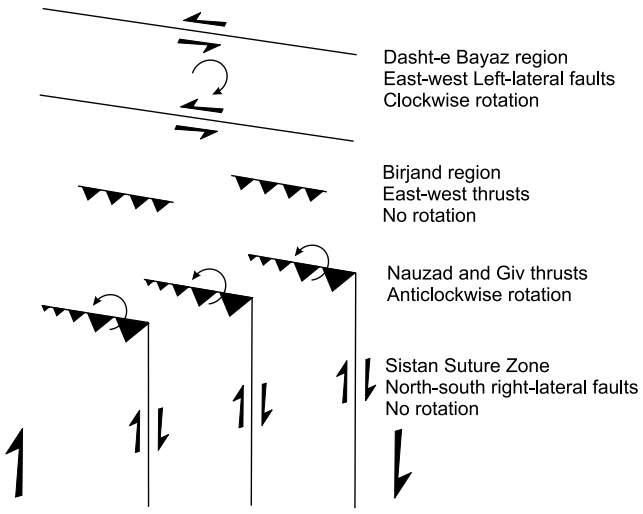

Figure 13. Schematic map of faulting in NE Iran. N-S right-lateral shear occurs across the entire region. In the south the shear is accommodated on N-S right-lateral faults of the Sistan Suture Zone. In the north, the shear is taken up on E-W left-lateral faults that rotate clockwise about vertical axes. The Giv and Nauzad thrusts link at their eastern ends with right-lateral faults of the Sistan Suture Zone and will probably rotate anticlockwise [e.g., *Bayasgalan et al.*, 1999a]. The rotating thrusts will allow the transition to the predominantly E-W thrust faulting near Birjand, which in turn are likely to be a consequence of clockwise vertical axis rotation of crustal material around the Dasht-e Bayaz fault in the north.

6.2. Influence of Preexisting Structure on Active Faulting

[38] One of the interesting questions leading from the model described in section 6.1 is why strain in northeast Iran should be accommodated by such a diffuse, and in places, complex pattern of faulting. To answer this, we must look at the relationship between the active faults and older geological structure.

[39] Each of the active faults described in section 5 show a close correlation with the location of old geological structures. Late Quaternary movement is seen along old ophiolitic shear zones running along the bedrock range fronts at both the northern and southern margins of the Rud-e Shur valley at Birjand (sections 5.2 and 5.3). The Nauzad fault along the Kuh-e Mo'inabad range front is parallel to the strike of bedrock lithologies (section 5.1). Other active faults are manifest at the Earth's surface as folding within alluvial and lake bed deposits. However, all of these folds are shown to be parallel to nearby mountainous regions exposing older geological structures. Furthermore, in each case, the folds overlie faults that dip toward these mountainous regions.

[40] For example, thrust faults underlying the Giv fold system south of Bagharan Kuh (section 5.6), are shown to dip toward the high topography of the mountains. The orientation of the folds show a close spatial correlation with the orientation of geological structures exposed in adjacent parts of Bagharan Kuh. In the western parts of the system, the folds strike roughly E-W, parallel to exposed structure within the mountains (e.g., Figures 2 and 4). Eastern parts of the fold system (between Mokhtaran and Sahlabad, Figure 2) trend NW-SE, again parallel to structures exposed within the mountains (the change in strike of both the folds and the exposed geology is visible in the bottom right corner of Figure 4).

[41] At Sahlabad, the Giv folds end in the N-S Esmailabad right-lateral strike-slip fault. The NW-SE geological structures are oblique to the Esmailabad fault at its northern end. However, south of Figure 2, both geological faults and rock units of the Sistan Suture Zone trend NNW-SSE to N-S [*Tirrul et al.*, 1983], and form a small angle with the active Esmailabad, Purang, and Neh faults (e.g., Figures 1 and 2). It therefore appears that the preexisting structure of the Birjand area exerts not only an influence on the topography of the region, but also on the patterns of active faulting, and hence the potential hazard from earthquakes.

[42] As discussed in section 6.1, the relatively diffuse pattern of faulting around Birjand is caused by the transition between two very different regimes of active faulting. This regional change from N-S right-lateral faulting, to left-lateral faulting within the E-W oriented ranges of northeastern Iran, also appears to result from a change in the preexisting regional structure [*Jackson and McKenzie*, 1984]. The Sistan Suture Zone, and the structures within it, trend roughly N-S along the eastern margin of the Dasht-e Lut. North of Birjand, the dominant geological structures trend E-W. This is seen within the mountain ranges of the Alborz and Kopeh Dagh (e.g., Figure 1). It is also seen with the presently inactive E-W

mountain ranges of northwest Afghanistan (e.g., Figure 1) [see also *Jackson and McKenzie*, 1984, Plate 6]. The influence of preexisting crustal weaknesses on patterns of active faulting may be one of the key reasons why the active faults in deforming zones do not always accommodate strain in the simplest way.

7. Conclusions

[43] The active faulting around Birjand is widespread and is presumably accommodating a change from right-lateral strike-slip faulting in the south of the study area, to left-lateral strike-slip faulting in the north, where the active deformation is thought to involve vertical axis clockwise rotation. As such, the diffuse pattern of faulting around Birjand is likely to be a consequence of the transition from rotational to nonrotational zones of deformation. The very low level of instrumental seismicity around Birjand is not likely to represent the full hazard from earthquakes.

[44] **Acknowledgments.** We would like to thank the University of Birjand and the Geological Survey of Iran in Tehran for their support and for enabling us to visit the region in 2004 and 2005. Golami and M. Zarrinkoub of the University of Birjand contributed to the fieldwork. Arabi was an excellent driver during fieldwork. We thank M. Berberian and an anonymous reviewer for constructive and detailed reviews. R.T.W. is supported by a NERC postdoctoral fellowship and by the NERC-funded Centre for the Observation and Modeling of Earthquakes and Tectonics (COMET).

References

Allen, M. B., R. Walker, J. Jackson, E. J.-P. Blanc, M. Talebian, and M. Ghassemi (2006), Contrasting styles of convergence in the Arabia-Eurasia collision: Why escape tectonics does not occur in Iran, *Mem. Geol. Soc. Am.*, in press.

Ambraseys, N. N., and C. P. Melville (1977), The seismicity of Kuhistan, Iran, *Geogr. J.*, *143*(2), 179–199.

Ambraseys, N. N., and C. P. Melville (1982), *A History of Persian Earthquakes*, Cambridge Univ. Press, New York.

Ambraseys, N. N., and J. S. Tchalenko (1969), The Dasht-e Bayaz (Iran) earthquake of August 31, 1968: A field report, *Bull. Seismol. Soc. Am.*, *59*, 1751–1792.

Bayasgalan, A., J. Jackson, J.-F. Ritz, and S. Carretier (1999a), Field examples of strike-slip fault terminations in Mongolia and their tectonic significance, *Tectonics*, *18*, 394–411.

Bayasgalan, A., J. Jackson, J.-F. Ritz, and S. Carretier (1999b), 'Forebergs', flower structures, and the development of large intracontinental strike-slip faults: The Gurvan Bogd fault system in Mongolia, *J. Struct. Geol.*, *21*, 1285–1302.

Berberian, M. (1976), Contribution to the seismotectonics of Iran (part II), *Rep. 39*, Geol. Surv. of Iran, Tehran.

Berberian, M. (1979), Earthquake faulting and bedding thrust associated with the Tabas-e-Golshan (Iran) earthquake of September 16, 1978, *Bull. Seismol. Soc. Am.*, *69*, 1861–1887.

Berberian, M., and R. S. Yeats (1999), Patterns of historical earthquake rupture in the Iranian plateau, *Bull. Seismol. Soc. Am.*, *89*, 120–139.

Berberian, M., and R. S. Yeats (2001), Contribution of archaeological data to studies of earthquake history in the Iranian plateau, *J. Struct. Geol.*, *23*, 563–584.

Berberian, M., J. A. Jackson, M. Qorashi, M. M. Khatib, K. Priestley, M. Talebian, and M. Ghafuri-Ashtiani (1999), The 1997 May 10 Zirkuh (Qa'enat) earthquake (M_w 7.2): Faulting along the Sistan suture zone of eastern Iran, *Geophys. J. Int.*, *136*, 671–694.

Berberian, M., J. A. Jackson, M. Qorashi, M. Talebian, M. M. Khatib, and K. Priestley (2000), The 1994 Sefidabeh earthquakes in eastern Iran: Blind thrusting and bedding-plane slip on a growing anticline, and active tectonics of the Sistan suture zone, *Geophys. J. Int.*, *142*, 283–299.

Camp, V. E., and R. J. Griffis (1982), Character, genesis and tectonic setting of igneous rocks in the Sistan suture zone, eastern Iran, *Lithos*, *3*, 221–239.

Eftekhar-Nezhad, J., and J. Stocklin (1992), Geological map of Iran sheet K8 (Birjand), scale 1:250,000, Geol. Surv. of Iran, Tehran.

Engdahl, E. R., R. van der Hilst, and R. Buland (1998), Global teleseismic earthquake relocation with improved travel times and procedures for depth determination, *Bull. Seismol. Soc. Am.*, *88*, 722–743.

England, P., and J. Jackson (1989), Active deformation of the continents, *Annu. Rev. Earth Planet. Sci.*, *17*, 197–226.

England, P., and P. Molnar (1990), Right-lateral shear and rotation as the explanation for strike-slip faulting in eastern Tibet, *Nature*, *344*, 140–142.

Farr, T. G., and M. Kobrick (2000), Shuttle Radar Topography Mission produces a wealth of data, *Eos Trans. AGU*, *81*(48), 583–585.

Freund, R. (1970), Rotation of strike slip faults in Sistan, southeast Iran, *J. Geol.*, *78*, 188–200.

Jackson, J. (2001), Living with earthquakes: Know your faults, *J. Earthquake Eng.*, *5*, 5–123, (Special Issue 1).

Jackson, J., and D. McKenzie (1984), Active tectonics of the Alpine-Himalayan Belt between western Turkey and Pakistan, *Geophys. J. R. Astron. Soc.*, *77*, 185–264.

Jackson, J. A., and P. Molnar (1990), Active faulting and block rotations in the Western Transverse Ranges, California, *J. Geophys. Res.*, *95*, 22,073–22,087.

LeStrange, G. (1905), *The Lands of the Eastern Caliphate*, Cambridge Univ. Press, New York.

McKenzie, D. (1972), Active tectonics of the Mediterranean region, *Geophys. J. R. Astron. Soc.*, *30*, 109–185.

McKenzie, D., and J. Jackson (1983), The relationship between strain rates, crustal thickening, palaeomagnetism, finite strain and fault movements within a deforming zone, *Earth Planet Sci. Lett.*, *65*, 182–202.

Meyer, B., P. Tapponnier, L. Bourjot, F. Metivier, Y. Gaudemar, G. Peltzer, G. Shunmin, and C. Zhitai (1998), Crustal thickening in Gansu-Qinghai, lithospheric mantle subduction, and oblique, strike-slip controlled growth of the Tibet Plateau, *Geophys. J. Int.*, *135*, 1–47.

Molnar, P., and P. Tapponnier (1975), Cenozoic tectonics of Asia: Effects of a continental collision, *Science*, *189*, 419–426.

Oskin, M., K. Sieh, T. Rockwell, G. Miller, P. Guptill, M. Curtis, S. McArdle, and P. Elliot (2000), Active parasitic folds on the Elysian Park anticline: Implications for seismic hazard in central Los Angeles, California, *Geol. Soc. Am. Bull.*, *112*, 693–707.

Parsons, B., T. Wright, P. Rowe, J. Andrews, J. Jackson, R. Walker, M. Khatib, M. Talebian, E. Bergman, and E. R. Engdahl (2006), The 1994 Sefidabeh (eastern Iran) earthquakes revisited: New evidence from satellite radar interferometry and carbonate dating about the growth of an active fold above a blind thrust fault, *Geophys. J. Int.*, *164*, 202–217, doi:10.1111/j.1365-246X.2005.02655.x.

Philip, H., and M. Meghraoui (1983), Structural analysis and interpretation of the surface deformation of the El Asnam earthquake of October 10, 1980, *Tectonics*, *2*, 17–49.

Philip, H., E. Rogozhin, A. Cisternas, J. C. Bousquet, B. Borisov, and A. Karakhanian (1992), The Armenian earthquake of 1988 December 7: Faulting and folding, neotectonics and palaeoseismicity, *Geophys. J. Int.*, *110*, 141–158.

Regard, V., et al. (2005), Cumulative right-lateral fault slip rate across the Zagros-Makran transfer zone: Role of the Minab-Zendan fault system in accommodating Arabia-Eurasia convergence in southeast Iran, *Geophys. J. Int.*, *162*, 177–203.

Schermer, E. R., B. P. Luyendyk, and S. Cisowski (1996), Late Cenozoic structure and tectonics of the northern Mojave Desert, *Tectonics*, *15*, 905–932.

Stein, R., and G. C. P. King (1984), Seismic potential revealed by surface folding: The 1983 Coalinga, California, earthquake, *Science*, *224*, 869–872.

Stein, R., and R. S. Yeats (1989), Hidden earthquakes, *Sci. Am.*, *260*, 48–57.

Talebian, M., and J. Jackson (2002), Offset on the Main Recent Fault of NW Iran and implications for the late Cenozoic tectonics of the Arabia-Eurasia collision zone, *Geophys. J. Int.*, *150*, 422–439.

Tirrul, R., I. R. Bell, R. J. Griffis, and V. E. Camp (1983), The Sistan suture zone of eastern Iran, *Geol. Soc. Am. Bull.*, *94*, 134–150.

Vernant, P., et al. (2004), Present-day crustal deformation and plate kinematics in the Middle East constrained by GPS measurements in Iran and northern Oman, *Geophys. J. Int.*, *157*, 381–398.

Walker, R. T. (2006), A remote sensing study of active folding and faulting in southern Kerman province, S.E. Iran, *J. Struct. Geol.*, *28*, 654–668.

Walker, R., and J. Jackson (2002), Offset and evolution of the Gowk fault, S.E. Iran: A major intra-continental strike-slip system, *J. Struct. Geol.*, *24*, 1677–1698.

Walker, R., and J. Jackson (2004), Active tectonics and late Cenozoic strain distribution in central and eastern Iran, *Tectonics*, *23*, TC5010, doi:10.1029/2003TC001529.

Walker, R., J. Jackson, and C. Baker (2003), Thrust faulting in eastern Iran: Source parameters and surface deformation of the 1978 Tabas and 1968 Ferdows earthquake sequences, *Geophys. J. Int.*, *152*, 749–765.

Walker, R., J. Jackson, and C. Baker (2004), Active faulting and seismicity of the Dasht-e-Bayaz region, eastern Iran, *Geophys. J. Int.*, *157*, 265–282.

M. M. Khatib, Department of Geology, Faculty of Sciences, Birjand University, Birjand, Iran. (mkhtib@birjand.ac.ir)

R. T. Walker, Department of Earth Sciences, University of Oxford, Parks Road, Oxford OX1 3PR, UK. (richard.walker@earth.ox.ac.uk)